

# Optical and photovoltaic properties of silicon wire solar cells with controlled ZnO nanorods antireflection coating

Seong-Ho Baek · Bum-Young Noh ·  
Jang-Kyoo Shin · Jae Hyun Kim

Received: 22 September 2011 / Accepted: 9 January 2012 / Published online: 21 January 2012  
© Springer Science+Business Media, LLC 2012

**Abstract** We introduce a new type of silicon micro-wire (SiMW) solar cell with a conformal zinc oxide (ZnO) nanorods anti-reflection coating (ARC) and discuss the optical and photovoltaic properties of the SiMW solar cells with controlled ZnO nanorods. The fabrication processes were composed of metal-assisted electroless etching combined with photolithography, spin-on-dopant diffusion, and hydrothermal synthesized ZnO nanorods growth. We found that the combination of Si wire geometry and ZnO ARC was able to maximize the light absorption and to minimize the light reflectance. Illuminated current–voltage ( $I$ – $V$ ) results show that the photovoltaic efficiency of SiMW solar cells with optimized ZnO ARC was enhanced more than 50% and the short-circuit current density was improved by over 43% compared to SiMW solar cells without ZnO ARC. This is mainly attributed to the reduced light reflectance and enhanced photon absorption. These hybrid structures are promising for making low-cost Si wire solar cells and making them applicable to photovoltaic devices with large areas.

## Introduction

Over the last few decades, there have been tremendous efforts to develop highly efficient photovoltaic systems

using organic [1], dye-sensitized [2, 3], and inorganic solid-state devices [4]. Among them, Si-based solar cells are the most dominant and occupy more than 80% of the total photovoltaic production market. However, solar cell efficiency still has not broken through the cost per watt hurdle, and cost remains a major concern to the widespread utilization of solar cells. Recently, nano and micro-structured three-dimensional (3D) Si has been attracting much attention for future applications in photovoltaic devices due to their superior properties [5–12]. Well-ordered wire arrays of Si have two major advantages relative to commercial crystalline and thin-film Si absorbers. First, p–n junctions in the radial direction enable minority carriers to drift only short distances to junction regions for efficient carrier collection. That means low grade Si raw materials can be utilized and manufacturing cost will be lowered [5]. In addition, the enhanced light absorption by ordered wire is attributed to the light trapping effect on the incident light [6, 7]. Moreover, a wire array transfer technique has been studied, which not only yields c-Si wires on a flexible substrate for photovoltaic applications, but also allows the c-Si wafer to be re-used for the further production of aligned wire arrays [10, 11].

For the fabrication of Si nano/micro structures, a number of bottom-up methods have been developed, such as vapor–liquid–solid (VLS) growth [8–11], chemical vapor deposition (CVD) [12], and molecular beam epitaxy (MBE) [13]. However, these growth processes have some disadvantages, as they generally need high temperature and high vacuum, or discharge toxic precursors. As an alternative top-down route, a few lithographic procedures, such as electron beam lithography [14], and reactive ion etching (RIE) [15] are widely used in Si-based fabrication processes, but they are expensive, time-consuming, and not suited for mass production of ordered nanostructures on a large-scale. In order

---

S.-H. Baek · B.-Y. Noh · J. H. Kim (✉)  
Division of Energy Research, Daegu Gyeongbuk Institute of  
Science & Technology (DGIST), 50-1, Sang-Ri, Hyeonpung-  
Myeon, Dalseong-gun, Daegu 711-873, Korea  
e-mail: jaehyun@dgist.ac.kr

S.-H. Baek · J.-K. Shin  
Department of Sensor and Display Engineering, Kyungpook  
National University (KNU), 80, Daehak Avenue, Buk-ku,  
Daegu, Korea

to overcome these problems, metal-assisted electroless etching has been attracting much interest due to the simple, large-scale, and cost-effective advantages [6, 7]. A thin layer of noble metal is deposited on the Si surface prior to immersion in a solution of hydrofluoric acid (HF) and hydrogen peroxide ( $\text{H}_2\text{O}_2$ ). Thin metal coatings facilitate etching in HF and  $\text{H}_2\text{O}_2$  and a reaction scheme involving local coupling of redox reactions can explain the metal-assisted electroless etching [16].

Also, a conventional antireflection layer is generally made by a quarter wavelength thickness dielectric layer. It reduces the reflectivity in a certain wavelength range via destructive interference of waves reflected from the top and the bottom of the ARC [17]. Recently, ZnO nanorods have been regarded as an efficient ARC, taking advantage of their good transparency, appropriate refractive index ( $n = 2$ ) and ability to form a textured coating via anisotropic growth [18, 19]. Chen and Sun [20] demonstrated that the light conversion efficiency was greatly enhanced by using the ZnO nanorod arrays as the AR layer on poly Si solar cells. However, the vertically aligned nanorod arrays were deposited on the surface of the planar solar cells. Even though there are many reports on the improvement of device performances by employing conformal ZnO coating on Si wire structures [21–23], most of the studies have been focused on the ZnO/Si heterojunctions rather than on ZnO ARC on Si wire solar cells.

In this study, we report the fabrication of vertical Si micro-wire (SiMW) solar cells with conformal ZnO nanorods ARC. And, the optical and photovoltaic properties of a SiMW solar cell with different size ZnO nanorods have been studied. The wire arrays of a c-Si were fabricated by means of metal-assisted chemical etching combining photolithography for site-selective etching. ZnO nanorods were grown on SiMW solar cells by using hydrothermal growth methods. To evaluate the cell performances, the p–n junction was prepared by an SOD diffusion method. The 3D hybrid architectures consisting of ZnO NWs and SiMW as reported in this study could take advantage of the inherent properties of both ZnO and Si with enlarged surface areas. Also, the combination of the Si wire geometry and ZnO nanorods ARC leads to enhanced light absorption and reduced light reflection across a broad spectral range.

## Experiments

### Fabrication of SiMW arrays

A p-type Si wafer with a resistivity of 1–10  $\Omega$  cm and (100) crystal orientation was used as a substrate. The Si wafers were cleaned in a boiled piranha solution of  $\text{H}_2\text{SO}_4/$

$\text{H}_2\text{O}_2$  (4:1, v/v) and RCA solution of  $\text{NH}_4\text{OH}/\text{H}_2\text{O}_2/\text{H}_2\text{O}$  (1:1:5, v/v) for 30 min, respectively. Then, wafers were washed in de-ionized water (DIW) for 10 min after being dipped in diluted hydrofluoric acid (DIW:HF = 50:1) to remove native oxide. The combination of photolithography and the catalytic Si etching technique was conducted in the following ways. First, the polished surface of Si wafer was coated with the positive photoresist (PR, AZ1512). Second, the PR was exposed to ultraviolet (UV) light through a photomask with predefined pattern. Third, the PR pattern for site-selective etching was obtained by development for 1 min with a develop solution. Fourth, 15-nm-thick gold (Au) thin film was deposited on the Si wafer by high-vacuum thermal evaporation. Fifth, ordered arrays of SiMW were produced on the surface of Si wafer after etching in aqueous HF solution (4.6 M) containing oxidizing agent (0.44 M) for 1 h. Finally, the remaining Au was thoroughly removed by immersing in conventional Au etchant at room temperature for 5 min.

### Synthesis of ZnO nanorods

ZnO nanorods were synthesized using two-step methods corresponding to the formation of seed layers and the growth of nanorods. The precursors used for ZnO synthesis are zinc acetate (99.99% purity, Aldrich Company), zinc nitrate (99.99% purity, Aldrich Company), and hexamethylenetetramine (HMT;  $\text{C}_6\text{H}_{12}\text{N}_4$ ). Hydrothermal growth of ZnO seed layers was performed by suspending the substrates perpendicular to the bottom of a beaker filled with an aqueous solution (25 mM) of zinc acetate and ethanol ( $\text{C}_2\text{H}_5\text{OH}$ ). Flat Si wafer and Si wire solar cells were used as substrates. Before introducing substrates into the growth solution, the precursor solution was coated on the substrates by dip-coating several times in a concentrated ethanol suspension at 70 °C. The substrates were then placed in a heated solution (25 mM) of zinc nitrate and HMT held at 85 °C. The growth time was varied over the range from 1 to 4 h with every 1 h, under otherwise nominally identical conditions, producing ZnO nanorods of increasing length. At the end of the growth period, the sample was removed from the solution, and immediately rinsed with DIW to remove residuals from the surface.

### Solar cell fabrication

A p–n junction was prepared by a solution processable SOD technique. To produce an n-type region, the phosphorus doped SOD solution (P509, Filmtronics) was spin-coated onto a dummy wafer and the sample was loaded in a conventional quartz-tube furnace at 1050 °C for 5 min while the target samples were kept at a closely spaced

distance. Phosphorosilica film was removed simply by immersing the prepared specimens in buffer oxide etchant (BOE) for 10 min. To verify the phosphorous diffusion, depth profiling of  $^{31}\text{P}$  was conducted with secondary ion mass spectrometry (SIMS, Cameca IMS-6f magnetic sector) using 15 kV  $\text{Cs}^+$  beam with a current of 90 nA. The thickness of the  $\text{n}^+$  emitter layer is approximately 510 nm. The active area of all devices was defined as  $1\text{ cm}^2$ . Indium/gallium eutectic metal (Ga (75%) In (25%) by weight, the melting point ( $\sim 15.5\text{ }^\circ\text{C}$ ) was used to form an electrical contact on both sides. Especially, the front contact was made using eutectic liquid metals with a gold probe tip on top of a wire array.

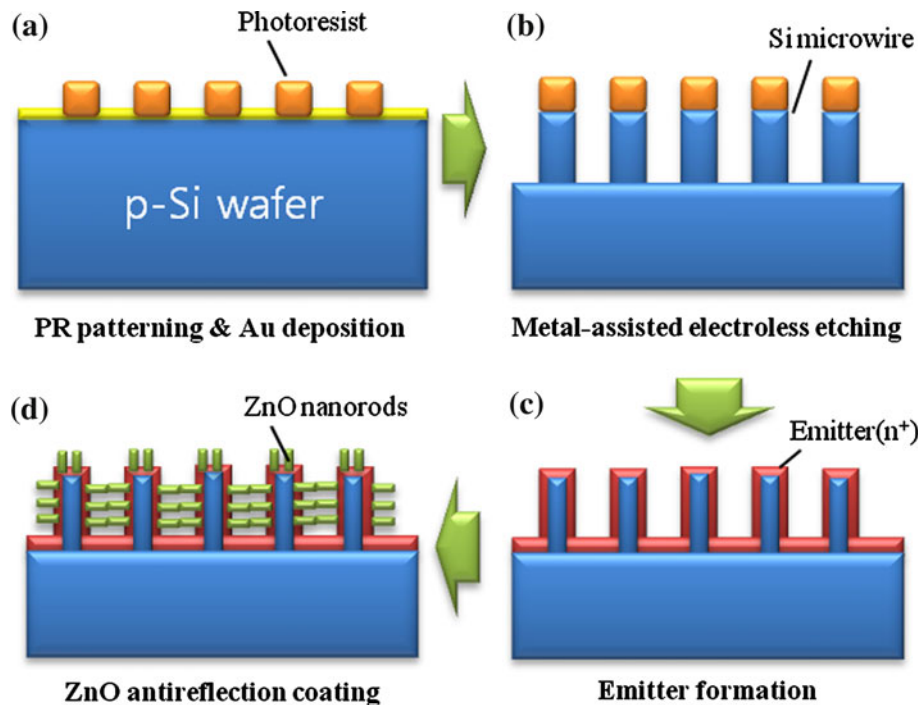
#### Characterization

The morphological properties of all the samples were characterized by scanning electron microscopy (SEM, Hitachi S-4800) and the optical properties of the fabricated wire arrays were measured from the ultraviolet to the infrared region using a spectrophotometer (Cary 500, Varian). Current–voltage ( $I$ – $V$ ) measurements were carried out with a source meter (Model 2400, Keithley) and with a Newport 91192 solar simulator system (equipped with 1 kW Xenon arc lamp from Oriol). The light intensity was adjusted to simulated AM 1.5 radiation at  $100\text{ mW/cm}^2$  with a radiant power energy meter (Model 70260, Oriol). Incident photon-to-current conversion efficiency (IPCE) results were acquired from an IPCE G1218a (PV measurement).

#### Results and discussion

Figure 1 shows the fabrication processes for making the array of ordered SiMW solar cells with ZnO ARC, which is described in detail in the experimental section. The prepared Si substrate was coated by a layer of approximately  $1\text{ }\mu\text{m}$  thick PR. The cured PR was then exposed in an i-line lithography setup with a 365 nm wavelength UV radiation for exposure. The exposed PR was removed by proper developing, leaving behind the unexposed PR circle on the substrate with the diameter of  $4\text{ }\mu\text{m}$ . The substrate was then subjected to an Au deposition and metal-assisted chemical etching, resulting in perfectly ordered SiMW arrays. It is clear that the site-selective redox reaction occurred only between the Au film and the exposed parts of the Si wafer, because Au thin film was used as a catalyst to etch pores into the Si wafer in the  $\text{HF-H}_2\text{O}_2$  solution. After galvanic reactions, the remaining Au film was removed by Au etchant, and the remaining PR was also eliminated by acetone to obtain periodically arranged Si wires, respectively. The geometry and the density of SiMW arrays could be controlled individually by varying the pattern size and etching parameters. Figure 2a–d shows the SEM images of SiMWs. The SiMW arrays were obtained uniformly over large areas. The cross-section SEM image reveals that the size of the SiMW is  $4\text{ }\mu\text{m}$  in diameter and  $12\text{ }\mu\text{m}$  in length, respectively, and Fig. 2c, d is the top-view images. The spacing between adjacent wires was kept at  $4\text{ }\mu\text{m}$  in both of the samples. In addition, the wire height could be well controlled by varying the etching durations.

**Fig. 1** Schematic illustration of the fabrication processes: **a** PR patterning and metal deposition. **b** Metal-assisted electroless etching. **c** Emitter formation. **d** ZnO antireflection coating



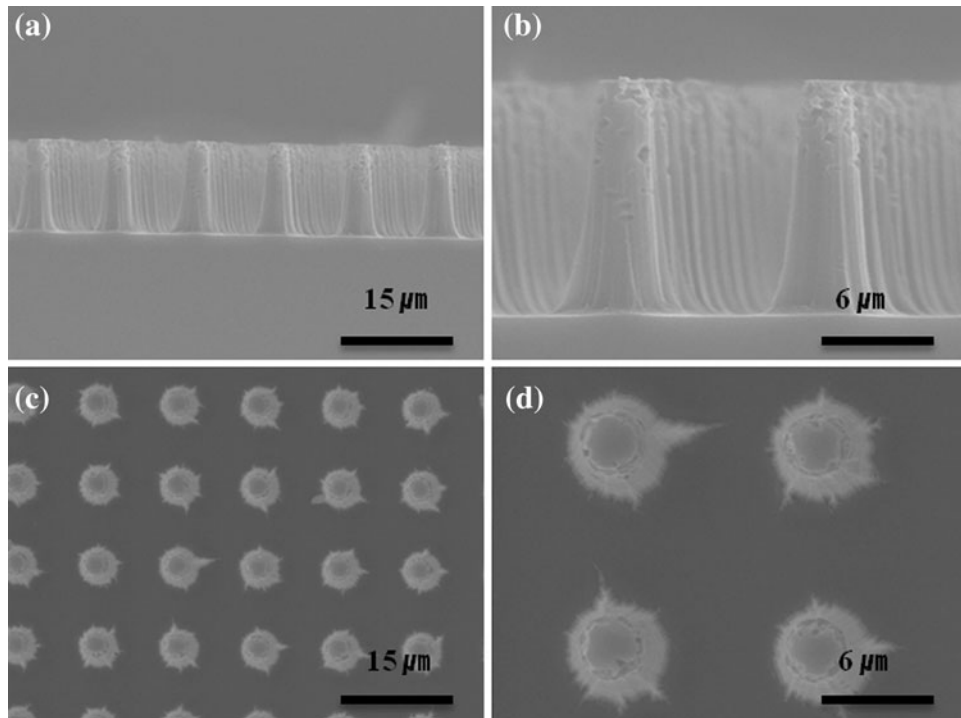


**Fig. 2** SEM images of the SiMW arrays: **a, b** cross sectional view; **c, d** top-view

To investigate the morphological properties of ZnO nanorods, we have synthesized vertically aligned ZnO nanorods on flat bare Si with solution methods using a two-step procedure. The ZnO seed layers were dip-coated

several times followed by the hydrothermal growth of ZnO nanorods. Figure 3 shows the SEM images of ZnO nanorods grown on a bare Si wafer by changing growth time from 1 to 4 h with every 1 h, respectively, while the other

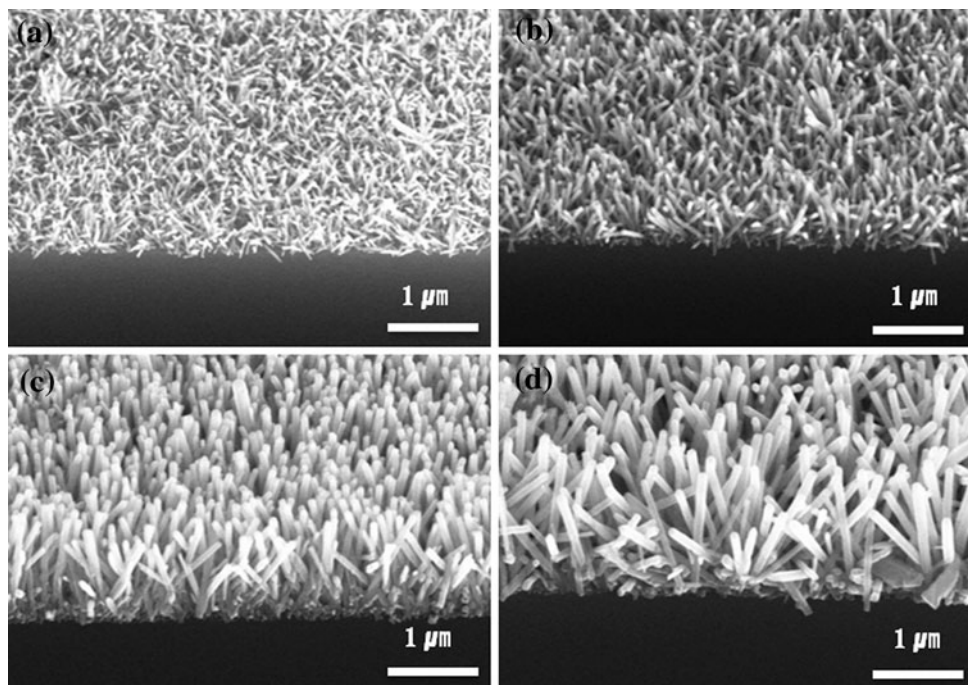


**Fig. 3** SEM images of the ZnO nanorods grown on flat bare Si wafer with growth time of **a** 1 h. **b** 2 h. **c** 3 h. **d** 4 h, respectively



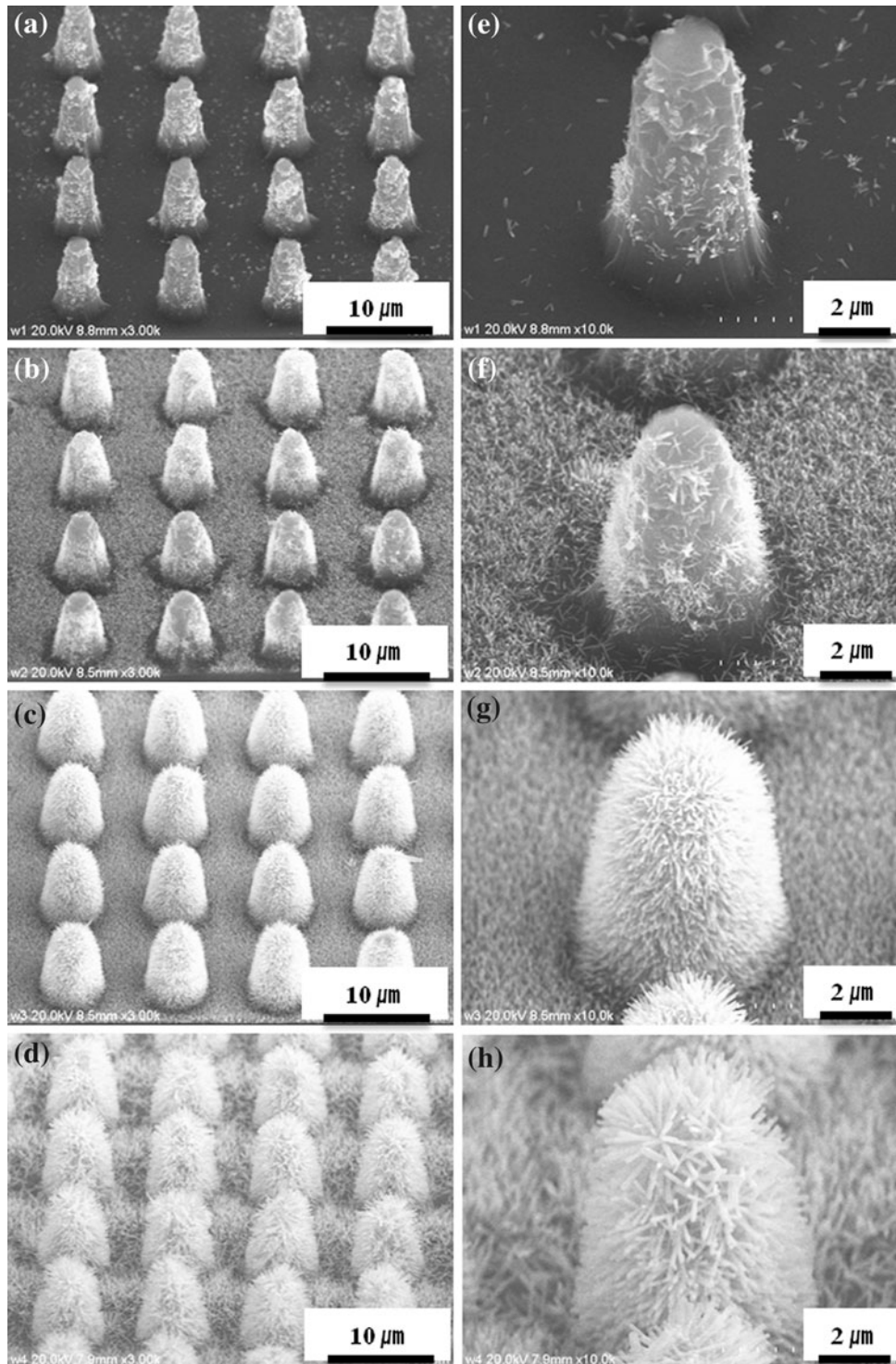


**Fig. 4** SEM images of the SiMW solar cells with ZnO nanorods ARC: **a** after 1 h of ZnO nanorods growth, **b** 2 h growth, **c** 3 h growth, **d** 4 h growth. High-magnification images of each sample are sequentially corresponding to **(e–h)**, respectively

etching parameters were kept constant. The size of the seed layer is about 20 nm (not shown). Figure 3a–d provides the SEM images of the growth of ZnO nanorods with time, which starts with the formation of the nanorods on the ZnO

seed layer. The arrays consisted of nanorods with diameters of 50–100 nm and the lengths of the rods were varied according to the growth time. The lengths of the nanorods were measured to be about 350, 545, 910 nm, and 1.25 μm,

respectively. We can also see that the size of the ZnO nanorods of each sample is uniform, and the hexagonal ZnO nanorods demonstrate good crystallinity. We observed that axial and radial growth occurred with increasing growth time and finally covered the whole Si surface after the grow time of 4 h.

Then, to investigate the properties of ZnO nanorods as an AR layer, ZnO arrays were incorporated on prepared SiMW solar cells. The SiMWs were employed as a template for the sequential growth of ZnO nanorods to construct a tree structure. Before that, SiMW solar cells were fabricated by n-type thermal doping on p-type Si wire arrays as illustrated in Fig. 1c. There are observable changes between the SiMW solar cell with ZnO nanorods and without them as shown in Fig. 4. We grew vertically aligned ZnO nanorods conformally on SiMW structures including the bottom of the Si surface area. At the beginning of synthesis, the ZnO nanorods were sparsely distributed on the surface of the Si wire and bottom areas (Fig. 4a). As growth time goes on, ZnO nanorods were densely grown on the Si wire surface in all directions, forming tree-like structures. In addition, ZnO nanorod arrays were directed normal to and along the Si wire surfaces just the same as those grown on bare Si substrates (Fig. 3). The high-magnification images of ZnO nanorods grown on SiMW solar cells corresponding to Fig. 4a–d are also given in Fig. 4e–h, respectively.

To study the optical properties of Si wire arrays and ZnO ARC, reflectance measurements were carried out using an integrating sphere. As shown in Fig. 5, the results demonstrate that the reflectance spectra of the SiMW solar cells with ZnO ARC were clearly lower than that of the cells without it over the wavelength range from ultraviolet to the near infrared region. Moreover, as the density and the size of ZnO nanorods were increased, the reflectance values were decreased. We suggest that the ZnO nanorods trap light, leading to suppressing light reflection and increasing light transmission to the SiMW solar cells. The reflectance ( $R$ ) is generally given by  $R = 1 - A - T$ , where

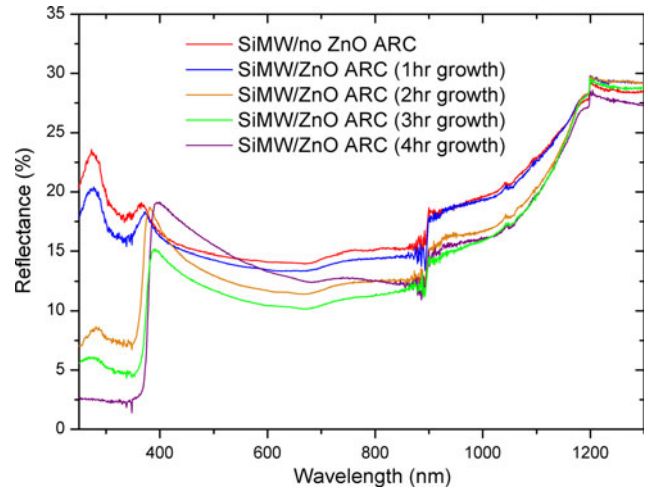
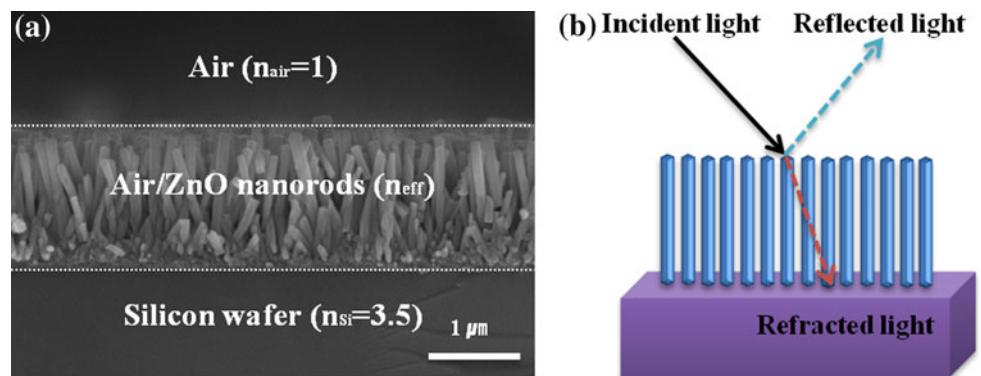


**Fig. 5** The reflectance spectra of the SiMW solar cells with and without ZnO nanorods ARC

$A$  is absorbance and  $T$  is transmittance. Therefore, a decrease in reflectance means an increase in absorbance and transmittance. As the transmittance is affected by sample thickness, it was ignored here due to the nearly unchanged thickness of the substrate after etching [24]. Thus, the possible reduction in reflectance may be caused by the increase in the absorbance using hybrid architectures consisting of ZnO nanorods and SiMWs. However, with the growth time of 4 h, SiMW solar cells with ZnO nanorods ARC showed enhanced reflectance values compared to those of other SiMW solar cells in the visible light range of spectrum. It is considered that the increased surface area of the ZnO nanorods reflects incident light to the opposite direction and impedes the light transmission to the Si wires [20].

In addition, the antireflection properties of uniformly distributed nanostructures are well described by the effective medium theory [25–27]. According to the effective medium theory, the effective refractive index ( $n_{\text{eff}}$ ) can be approximated by  $n_{\text{eff}} = [f_{\text{ZnO}} \times n_{\text{ZnO}}^{2/3} + f_{\text{air}} \times n_{\text{air}}^{2/3}]^{3/2}$ , where  $n_{\text{ZnO}}$  and  $n_{\text{air}}$  are the refractive index of ZnO and air

**Fig. 6 a** Effective refractive index profiles of ZnO ARC on Si wafer and **b** schematic diagram of the light path



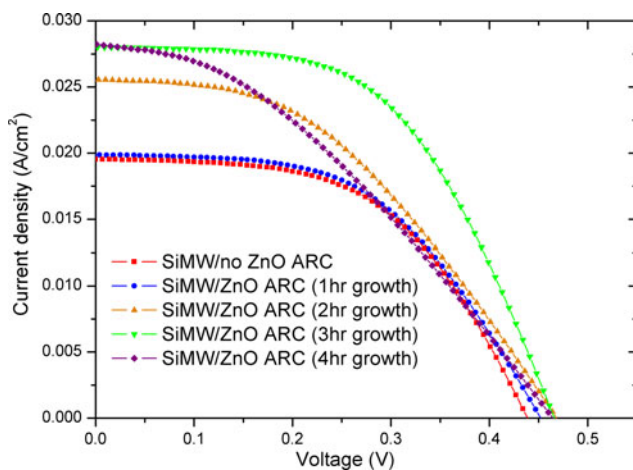


**Fig. 7** The light current density–voltage ( $J$ – $V$ ) characteristics of the SiMW solar cells with and without ZnO nanorods ARC

at wavelength of 600 nm, respectively. The  $f$  is the volume fraction of each material. Effective refractive index profiles of ZnO ARC on Si wafer and a schematic diagram of the light path is described in Fig. 6. In the case of SiMW solar cells without ZnO ARC, the reflectance was significantly higher because of its large index difference between air ( $n_{\text{air}} \approx 1$ ) and Si material ( $n_{\text{Si}} \approx 3.5$ ). When increasing the growth time of ZnO ARC, the  $n_{\text{eff}}$  was also linearly increased, resulting in considerably reduced reflectance and enhanced refraction. However, further increases in growth time up to 4 h gave rise to denser ZnO nanorods with higher  $n_{\text{eff}}$ , which can greatly enhance the surface reflection from the incident light due to the large index difference between air and the ZnO nanorods layer. On the other hand, the decreased reflectance values around 380 nm wavelength were observed for all the grown ZnO nanorods samples. This is attributed to the band edge absorption of ZnO nanorods, strongly increased with the size and the density of ZnO nanorods [23].

The current density–voltage ( $J$ – $V$ ) characteristics of the SiMW solar cells with and without ZnO ARC were observed under  $100 \text{ mW/cm}^2$  of simulated AM 1.5 G illumination. We found that good agreement between reflectance spectra and cell performances can be achieved through an introduction of the ZnO ARC. From the  $J$ – $V$  curves as depicted in Fig. 7, we observed that the cell performances were greatly improved with the increasing density and size of ZnO nanorods until the growth time of 3 h. SiMW solar cells with optimized ZnO nanorods ARC (green scatter) yielded the best performance with an open circuit voltage ( $V_{\text{oc}}$ ) of 466 mV, a short circuit current ( $J_{\text{sc}}$ ) of  $27.9 \text{ mA/cm}^2$ , a fill factor (FF) of 54%, and a cell efficiency (CE) of 7%. For the SiMW solar cell with optimized ZnO ARC, the light conversion efficiency was increased

**Table 1** The photovoltaic properties of the SiMW solar cells

Samples	$V_{\text{oc}}$ (mV)	$J_{\text{sc}}$ ( $\text{mA/cm}^2$ )	FF (%)	$\eta$ (%)
Without ZnO ARC	438	19.5	53.7	4.6
With ZnO ARC (1 h growth)	452	19.8	52.2	4.69
With ZnO ARC (2 h growth)	468	25.5	49.4	5.75
With ZnO ARC (3 h growth)	466	27.9	53.9	7.04
With ZnO ARC (4 h growth)	464	28.2	50.4	4.76

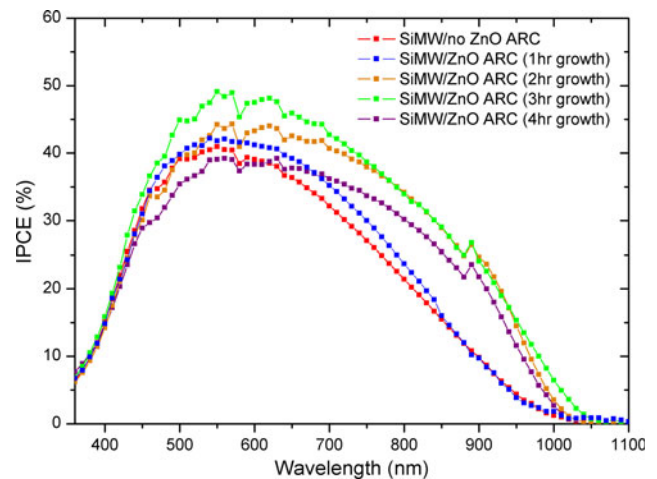


**Fig. 8** IPCE spectra of the SiMW solar cells with and without ZnO ARC

from 4.6 to 7%, indicating an approximate 50% improvement of the total energy conversion efficiency compared to the cell without AR treatment (red scatter). This is mainly caused by the reduced light reflection and enhanced photon absorption using ZnO ARC. For nanostructured surfaces, the surface morphology exhibiting arrayed nanorods improved the photovoltaic conversion efficiencies due to the enhanced absorption caused by multiple scatterings. However, when the growth time of ZnO nanorods approached 4 h, the photovoltaic performances drastically deteriorated. As mentioned above, we suggest that the excessively enlarged ZnO nanorods increase the light reflectance and disturb the light absorption to the SiMWs. Table 1 summarizes the photovoltaic performance of the SiMW solar cells with and without ZnO ARC, respectively.

Finally, the IPCE spectra of the SiMW solar cells with and without ZnO ARC are compared in Fig. 8. The origin of the increased  $J_{\text{sc}}$  of SiMW with ZnO ARC was clearly revealed by the results of enhanced IPCE. The IPCE curves display results that are consistent with the trend in  $J_{\text{sc}}$ , and SiMW solar cell with ZnO ARC showed higher IPCE than that of the cell without it. The increased IPCE across a broad spectral range could be attributed to the reduced

reflection and enhanced photon absorption by ZnO nanorods coated SiMWs. However, it is remarkable that the IPCE result of the SiMW solar cells with the ZnO growth time of 4 h were drastically reduced compared to those of other SiMW solar cells with ZnO ARC due to the enhanced surface reflection.

## Conclusions

We fabricated the SiMW solar cells with different sizes of ZnO nanorods ARC and characterized their optical and photovoltaic properties. With an increasing density and size of ZnO nanorods, the reflectance values decreased by suppressing light reflection and increasing light transmission to the SiMW solar cells. The photovoltaic efficiency of the SiMW solar cells with optimized ZnO ARC was also enhanced more than 50% and  $J_{sc}$  was improved by over 43% compared to ZnO AR uncoated SiMW solar cells. The 3D hybrid structures, i.e., SiMW solar cell with ZnO ARC, are a promising alternative for solar energy harvesting devices.

**Acknowledgements** This study was financially supported by the Pioneer Research Center Program through the National Research Foundation of Korea (2011-0001649) and by a basic research program (11-EN-03) through the Daegu-Gyeongbuk Institute of Science and Technology (DGIST) funded by the Ministry of Education, Science and Technology (MEST).

## References

- Huynh WU, Dittmer JJ, Alivisatos AP (2002) *Science* 295:2425
- Grätzel M (2001) *Nature* 414:338
- Law M, Greene LE, Johnson JC, Saykally R, Yang PD (2005) *Nat Mater* 4:455
- Chamberlain GA, Cooney PJ, Dennison S (1981) *Nature* 289:45
- Kayes BM, Atwater HA, Lewis NS (2005) *J Appl Phys* 97:114302
- Peng K, Xu Y, Wu Y, Yan Y, Lee ST, Zhu J (2005) *Small* 1:1062
- Garnett EC, Yang P (2008) *J Am Chem Soc* 130:9224
- Tian B, Zheng X, Kempa TJ, Fang Y, Yu N, Yu G, Huang J, Lieber CM (2007) *Nature* 449:885
- Stelzner T, Pietsch M, Andra G, Falk F, Ose E, Christiansen S (2008) *Nanotechnology* 19:295203
- Putnam MC, Boettcher SW, Kelzenberg MD, Turner-Evans DB, Spurgeon JM, Warren EL, Briggs RM, Lewis NS, Atwater HA (2010) *Energy Environ Sci* 8:1037
- Kayes BM, Filler MA, Putnam MC, Kelzenberg MD, Lewis NS, Atwater HA (2007) *Appl Phys Lett* 91:103110
- Tsakalacos L, Balch J, Fronheiser J, Korevaar BA, Sulima O, Rand J (2007) *Appl Phys Lett* 91:233117
- Fuhrmann B, Leipner HS, Höche H, Schubert L, Werner P, Gösele U (2005) *Nano Lett* 5:2524
- Ng H, Han J, Yamada T, Nguyen P, Chen Y, Meyyappan M (2004) *Nano Lett* 4:1247
- Huang M, Yang C, Chiou Y, Lee R (2008) *Sol Energy Mater Sol Cells* 92:1352
- Qiu T, Chu RK (2008) *Mater Sci Eng R* 62:59
- Chhajer S, Schubert MF, Kim JK, Schubert EF (2008) *Appl Phys Lett* 93:251108
- Lee YJ, Ruby DS, Peters DW, McKenzie BB, Hsu JW (2008) *Nano Lett* 8:1501
- Chao YC, Chen CY, Lin CA, Dai YA, He JH (2010) *J Mater Chem* 20:8134
- Chen JY, Sun KW (2010) *Sol Energy Mater Sol Cells* 94:930
- Sun K, Jing Y, Park N, Li C, Bando Y, Wang D (2010) *J Am Chem Soc* 132:15465
- Um HD, Moiz SA, Park KT, Jung JY, Jee SW, Ahn CH, Kim DC, Cho HK, Kim DW, Lee JH (2011) *Appl Phys Lett* 98:033102
- Song HS, Zhang WJ, Cheng C, Tang YB, Luo LB, Chen X, Luan CY, Meng XM, Zapfen JA, Wang N, Lee CS, Bello I, Lee ST (2011) *Cryst Growth Des* 11:147
- Kong BH, Choi MK, Cho HK, Kim JH, Baek SH, Lee JH (2010) *Electrochem Solid-State Lett* 13:12
- Tinga WR, Voss WAG, Blossey DF (1973) *J Appl Phys* 44:3897
- Li H, Jiang B, Schaller R, Wu J, Jiao J (2010) *J Phys Chem C* 114:11375
- Ko YH, Leem JW, Yu JS (2011) *Nanotechnology* 22:205604